

A Synergy Scoring Filter for Unsupervised Anomaly Detection with Noisy Data

Fengjie Wang Chengming Liu Pang Haibo Lei Shi
 Zhengzhou University
 oo.ggg42@gmail.com
 {cmliu, phb, shilei}@zzu.edu.cn

Abstract

Noise-inclusive fully unsupervised anomaly detection (FUAD) holds significant practical relevance. Although various methods exist to address this problem, they are limited in both performance and scalability. Our work seeks to overcome these obstacles, enabling broader adaptability of unsupervised anomaly detection (UAD) models to FUAD. To achieve this, we introduce the Synergy Scoring Filter (SSFilter), the first fully unsupervised anomaly detection approach to leverage sample-level filtering. SSFilter facilitates end-to-end robust training and applies filtering to the complete training set post-training, offering a model-agnostic solution for FUAD. Specifically, SSFilter integrates a batch-level anomaly scoring mechanism based on mutual patch comparison and utilizes regression errors in anomalous regions, alongside prediction uncertainty, to estimate sample-level uncertainty scores that calibrate the anomaly scoring mechanism. This design produces a synergistic, robust filtering approach. Furthermore, we propose a realistic anomaly synthesis method and an integrity enhancement strategy to improve model training and mitigate missed noisy samples. Our method establishes state-of-the-art performance on the FUAD benchmark of the recent large-scale industrial anomaly detection dataset, Real-IAD. Additionally, dataset-level filtering enhances the performance of various UAD methods on the FUAD benchmark, and the high scalability of our approach significantly boosts its practical applicability.

1. Introduction

Image anomaly detection can be broadly categorized into semantic anomaly detection and sensory anomaly detection [45]. Semantic anomaly detection emphasizes the overall semantics of the image, while sensory anomaly detection focuses on fine-grained details, such as small scratches on objects. This paper concentrates on sensory anomaly detection, which is already widely used in fields like intelligent manufacturing, lesion detection, and video surveil-

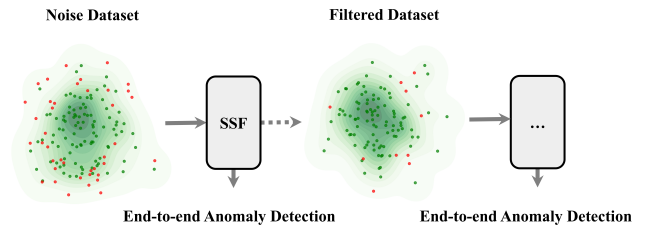


Figure 1. Filter the entire dataset using the trained SSFilter, extending to various other UAD methods.

lance. Due to the difficulty of obtaining anomalous samples, the unsupervised paradigm of training with only normal samples has gained great favor. However, as the scale increases, selecting a perfectly normal sample dataset still requires significant labor and time costs. Additionally, missed anomalies during screening can degrade model performance. Therefore, accounting for a certain level of noisy samples within the training set holds substantial practical relevance. Moreover, in sensory anomaly detection, the high similarity between normal and abnormal samples makes the subtle sensory contamination fundamentally different from the more pronounced semantic contamination commonly addressed in conventional noisy learning.

Existing unsupervised anomaly detection methods are generally categorized into three mainstream approaches: reconstruction-based methods [8, 14, 17, 42, 53], anomaly synthesizing-based methods [30, 46, 50, 52], and embedding-based methods [7, 38]. Since these methods assume a clean training set, their performance degrades when confronted with noisy data. PatchCore [38] is a foundational approach that extracts patch-level feature embeddings of normal images into a Memory Bank, detecting anomalous patches during inference through a patch query process. Recently, SoftPatch [21], building on PatchCore [38], introduced a patch-level filtering strategy where patch features are filtered and weighted before being stored in the Memory Bank to reduce contamination from anomalous patches, thereby enhancing model robustness. However, the improvement in performance remains limited, and the pro-

posed patch-level filtering strategy is not easily extendable to other methods.

To address this issue, we developed a highly scalable and high-performance robust training method with strong sample-level filtering capabilities. This method can independently conduct end-to-end training and directly perform sample-level filtering on the training set post-training, allowing other methods to benefit easily, as illustrated in the overall concept diagram in Figure 1. Specifically, drawing inspiration from advanced zero-shot batch-level anomaly detection techniques [5, 25], we designed an efficient in-batch sample filtering mechanism. The core principle is that anomalous patches exhibit higher sparsity and specificity, whereas normal patches are densely distributed and interconnected, enabling mutual scoring of patches. Anomalous patches, which lack similar counterparts, receive higher anomaly scores. This approach allows us to obtain anomaly scores for samples within the batch, filtering out high-risk samples to mitigate the noise’s impact on the model during iterative training.

However, this scoring strategy, as a zero-shot approach without training, introduces inherent biases. To mitigate the model’s over-reliance on such biases, we incorporate uncertainty estimation [10] and perform fine-grained, sample-level uncertainty estimation based on regression (reconstruction) errors and prediction uncertainty in anomalous regions. This uncertainty score serves as a corrective factor in the filtering process. Additionally, to address inevitable omissions, we developed a realistic anomaly synthesis method using by-products from uncertainty estimation and implemented a “restoring the hidden truth” strategy to guide model training and counteract anomalous interference.

Our method achieved state-of-the-art (SOTA) performance on the fully unsupervised benchmark of the latest large-scale industrial anomaly detection dataset, Real-IAD [41]. Additionally, our dataset-level filtering approach enhances fully unsupervised performance across various methods, supporting effective method selection for real-world applications. In summary, our contributions are as follows:

- To the best of our knowledge, our proposed SSFilter method is the first sample-level filtering-based approach for fully unsupervised anomaly detection. Its exceptional scalability and performance significantly bridge the gap between fully unsupervised anomaly detection and traditional unsupervised anomaly detection.
- We proposed a sample-level filtering strategy based on the synergy of patch mutual scoring and uncertainty estimation, which performs excellently.
- We proposed a realistic anomaly synthesis method, upon which we built a “restoring the hidden truth” strategy to enhance model performance.

2. Related Work

2.1. Unsupervised Anomaly Detection

Reconstruction. Reconstruction-based methods operate on a fundamental assumption: during training, normal images are accurately reconstructed, while during inference, anomalous regions fail to reconstruct due to the model’s lack of exposure to these patterns. Early models focused on pixel-level reconstruction, but they often produced sub-optimal results [2, 11, 28, 33]. Recently, researchers have aimed to enhance reconstruction quality by decoupling image frequencies [27] or employing advanced diffusion models [31]. In parallel, many recent studies, inspired by knowledge distillation [18], have shifted their focus to feature-level reconstruction. Reverse Distillation (RD) [8] has become popular due to its efficient and simple structure, and numerous innovative improvements [14, 39, 39, 42] have been developed based on it. For example, [14] explored extending RD to Vision Transformers [9], proposing key elements such as loose reconstruction, noise bottlenecks, and linear attention [23], all of which play a significant role.

Synthetic Anomaly. Methods that synthetic anomalies provide valuable supervisory signals by generating synthetic anomalies. For example, CutPaste [24] creates anomalies through random cutting and pasting, while DRAEM [50] applies Perlin noise and an auxiliary texture dataset to generate anomalies. DeSTSeg [51] uses a similar anomaly synthetic strategy in conjunction with feature reconstruction methods. Additionally, SimpleNet introduces Gaussian noise in the feature space to simulate anomalies. However, the generalization of these synthetic anomaly methods is limited.

Zero/few-shot. The development of visual-language models (VLMs) has significantly advanced zero/few-shot anomaly detection. For example, [20, 54] achieved both zero-shot and few-shot anomaly detection using the VLM model CLIP. Additionally, researchers leveraged the characteristics of sensory anomaly detection—where normal image patches find many similar patches in other unlabeled images, while anomalous patches find few—and proposed a mutual scoring strategy for images [5, 25]. This approach supports few-shot anomaly detection without VLMs and can extend to zero-shot anomaly detection within batches.

2.2. Learning with Noisy Data

Learning with Noisy Labels (LNL) and Semi-Supervised Learning (SSL) have gained significant attention for their practical applications. Some studies [29, 40, 47] suggest that label noise distribution is learnable, allowing labels to be restored by modeling this distribution. [19] uses loss values from multiple training rounds as a basis for sample selection. Other researchers [15, 43] mitigate the impact of noise through information exchange and fusion between

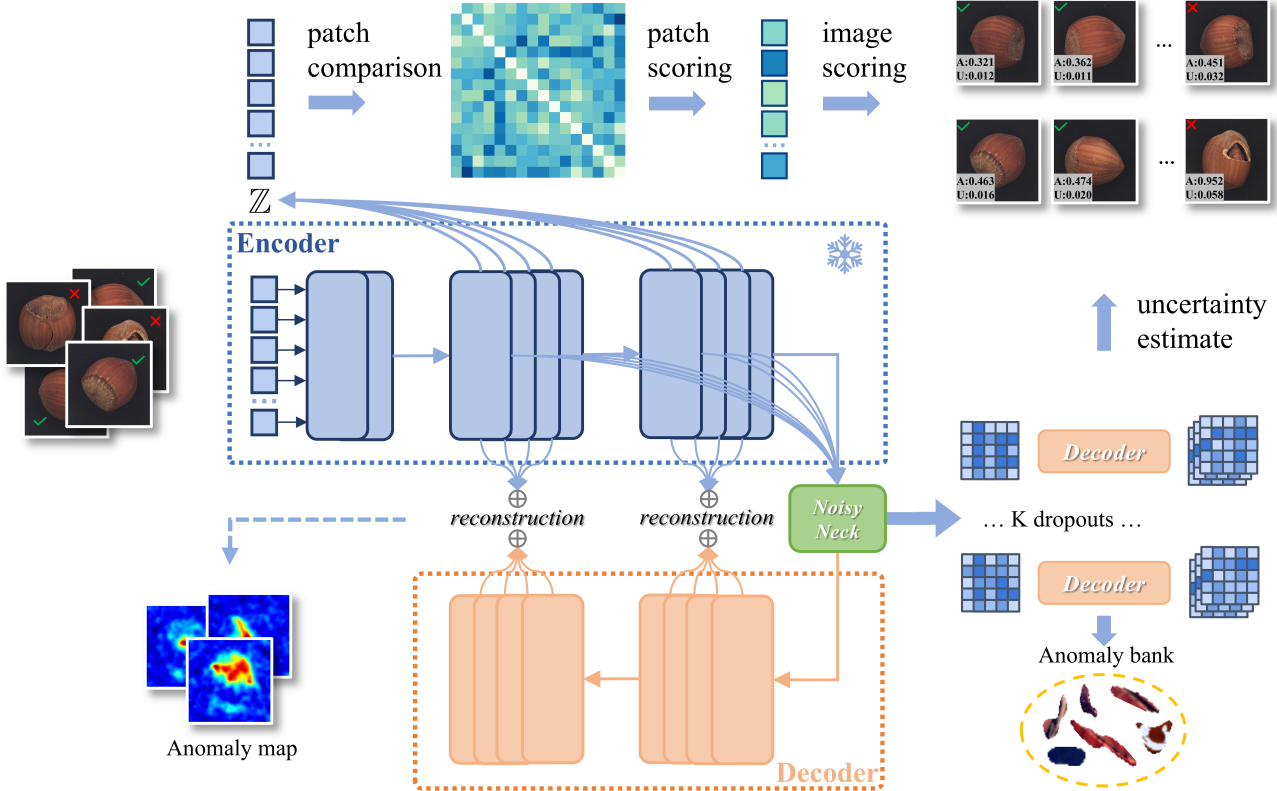


Figure 2. The overall framework of SSFilter. The patch comparison scorer and uncertainty estimator work synergistically to filter high-risk samples in the batch.

multiple homogeneous models. In SSL, UPS [37] applies MC-Dropout [10] to estimate prediction uncertainty, which helps correct model output and select more reliable pseudo-labels.

However, adding noise in unsupervised sensory anomaly detection [45] introduces new challenges, as there are no reliable samples for model calibration, and normal and anomalous samples in sensory AD are difficult to distinguish. Additionally, sensory contamination in reconstruction models can directly cause “identical shortcuts” [49], leading to substantial model contamination. To address these issues, many existing methods [3, 35, 48] continue to apply semantic AD approaches to sensory AD, leading to a significant performance gap when compared to state-of-the-art sensory AD methods that do not incorporate Noisy. Recently, SoftPatch [22], based on PatchCore [38], proposed a patch-level filtering strategy that first filters out some anomalous patches, then stores them in a weighted Memory Bank, where each patch’s anomaly score is calculated based on the distance to its nearest patch during inference. Although this method narrows the performance gap, its scalability and effectiveness remain limited.

3. Method

Figure 2 shows the overall framework of the SSFilter. In the following sections, we introduce the components of SSFilter. Section 3.1 presents our improved baseline model. Section 3.2 describes an efficient batch filter based on patch-wise comparative scoring. In Section 3.3, we introduce a fine-grained uncertainty estimator that detects subtle anomalies in noisy images by leveraging uncertainty awareness. As discussed in Section 3.4, we integrate these two filtering mechanisms to create a robust sample-level noise filter. Despite these efforts, indistinguishable noisy data can still interfere with the model, causing it to learn abnormal patterns. To address this, Section 3.5 proposes an integrity enhancement scheme that recovers normal features from realistically generated synthetic anomalies to guide the model and counter overlooked anomalies. Finally, in Section 3.6, we present a method for scaling a well-trained model to dataset-level filtering.

3.1. Dinomaly with Enhancing Linear Attention

Our baseline model incorporates Dinomaly [14], a reconstruction model with strong performance, using DINOv2 [6, 32] as the encoder. DINOv2 provides powerful patch

feature representation capabilities, which are essential for the comparative scoring filter. The original Dinomaly extends the RD framework to Vision Transformers, featuring an encoder, a noise bottleneck, and a linear attention [23] decoder. Their experiments show that linear attention’s “non-focusing ability” enhances the reconstruction model’s performance. However, a prevailing view is that linear attention lacks expressive capacity [4, 34], which limits decoder effectiveness. To address this, we incorporate Mamba-Like Linear Attention (MLLA) [16], an enhanced form of linear attention inspired by Mamba [12]. MLLA integrates key elements of Mamba into linear attention, yielding strong performance improvements.

3.2. Patch Comparison Scoring

It is widely accepted that anomalies are outliers, characterized by their specificity and rarity. The concept of mutual scoring between image patches within a batch [25] builds on this notion. In essence, it assumes that normal image patches can find several similar patches within a batch, while anomalous patches are difficult to match. Its performance depends on two core components: the patch feature descriptor and the mutual scoring strategy.

Patch Feature Descriptor. We leverage DINOv2 as a powerful feature extractor, with the output of each ViT block naturally serving as a Patch Feature Descriptor. We denote $\phi_{i,j} = \phi_j(x_i) \in \mathbb{R}^{N \times C}$ as the feature embedding of image x_i at the j -th layer of the pretrained network ϕ , where N is the number of patches and C is the feature dimension.

Following the guidance of previous studies [7, 26, 38], selecting middle-level features is crucial, as deeper feature embeddings tend to lose the local features that are critical for describing a relatively independent patch. To combine features from different levels, $\phi_{i,j}$, we concatenate them along the feature dimension. In addition to single-layer descriptions, we also concatenate averaged features from multiple levels to obtain a more comprehensive representation. In summary, features from different levels combine complementary information, mitigating the limitations of single-layer features. We define this process as:

$$z^i = f_{cat}(\{\phi_{i,l} | l \in L_1\}, \text{mean}(\{\phi_{i,l} | l \in L_2\})). \quad (1)$$

Mutual Scoring Strategy. Most advanced batch zero-shot anomaly detection methods require extended inference times. For both MuSc [25] and AnomalyDINO [5], the inference time for a single image on an RTX 3090 GPU exceeds 100ms, making it challenging to use them directly as batch-level filters during training. To address this, we simplify the process in the following steps: first, we use a single matrix multiplication operation to compute the mutual similarity of all patches within the mini-batch. Second, for each patch, we calculate the average distance of the top 0.1%

Algorithm 1 PyTorch-style pseudocode for patch comparison scoring.

```
# x - minibatch of images [B, C, H, W]
# N - total patch count, value BxHxW
# D - feature dimensions of patch descriptors
#
# mean - mean value function
# topk - function that takes the k largest values.

# compute patch feature descriptor
z = f(x) # [N, D]
# normalized feature embedding
z_norm = z / z.norm(dim=1)
# calculate the similarity matrix of patches
sims = z_norm @ z_norm.T # [N, N]
# fill in the diagonal
fill_diagonal_blocks(sims, HxW, 0)
# calculate the patch-level anomaly score # [N,]
p_s = 1 - mean(topk(sims, k=N * 0.001, dim=1), dim=1)
p_s = p_s.view(B,H*W) # [B, H*W]
# calculate the image-level anomaly score # [B,]
i_s = mean(topk(p_s, k=H * W * 0.01, dim=1), dim=1)
```

most similar patches, which serves as the final normalcy score for that patch. Finally, similar to the operation in many UAD algorithms that compute anomaly values from anomaly maps [5, 13, 14], we compute the average anomaly score of the top 1% most anomalous regions to obtain the image-level anomaly score a_i . The core pseudocode of the mutual scoring method is presented in Algorithm 1.

3.3. Awareness of Uncertainty

Since the patch scoring mechanism is an untrained zero-shot method, its performance is inherently constrained. To mitigate over-reliance on this approach, we propose a fine-grained, uncertainty-aware method. Specifically, we leverage the uncertainty caused by anomalous regions to refine the patch scoring mechanism. Furthermore, we extract real anomalous content from cumulative errors to generate realistic synthetic anomalies.

Uncertainty Estimate. Formally, let $F_i, \hat{F}_i \in \mathbb{R}^{C \times H \times W}$ represent the feature maps output by the encoder and decoder for the i -th image, where C , H , and W denote the channel count, height, and width of the output feature map, respectively. To estimate fine-grained uncertainty, the stacked decoder does not directly generate noise to avoid significant contamination of the alignment feature maps. Instead, we apply dropout K times at the noise bottleneck to generate K masked models. The anomalous images generated during each forward pass are as follows:

$$M_i^k = \mathcal{D}_M(F_i, \hat{F}_i, W^k). \quad (2)$$

where W^k denotes the weights of the k -th masked model, and \mathcal{D}_M represents a feature alignment function that generates anomaly maps. The anomaly score is computed as the mean of the maximum value regions:

$$s_i^k = \max_{0.01} (M_i^k). \quad (3)$$

The prediction uncertainty u_i of x_i is given by the standard deviation of $s_i \in \mathbb{R}^k$

Anomalous Material Extraction. Anomalous regions exhibit both high regression error and high prediction uncertainty, allowing us to extract anomalous material from anomaly samples. By combining stable foreground estimation, we can synthesize realistic anomalous samples. We accumulate K anomalous images as follows:

$$M_i^{acc} = \sum_{k=1}^K M_i^k. \quad (4)$$

This anomaly map accumulates both regression error and prediction uncertainty. Using a threshold, we crop the most anomalous regions as anomaly material, as shown in Figure 2.

3.4. Synergy Scoring Filtering

Since reliable uncertainty estimation relies on good reconstruction ability, we divide the training process into two main phases: the cold-start phase and the regular training phase. By default, the cold-start phase corresponds to the first 1,000 iterations of training.

Cold Start Phase. Since anomalous samples are present during training in the FUAD setting, our goal is to minimize the impact of these anomalies to improve performance. In the cold-start phase, the results from patch comparison scoring will serve as our primary reference. Since anomaly levels vary across different sample categories and sizes, applying a fixed threshold for filtering becomes challenging. Therefore, we employ a general filtering strategy, ranking the samples in a mini-batch and selecting the top half with high confidence for training. Formally, given a sorted set of anomaly scores $A' = \{a'_1, a'_2, \dots, a'_n\}$, where $a'_1 \leq a'_2 \leq \dots \leq a'_n$, we split the data into two subsets A'_1 and A'_2 as follows:

$$A'_1 = \{a'_1, a'_2, \dots, a'_m\}, \quad A'_2 = \{a'_{m+1}, a'_{m+2}, \dots, a'_n\}. \quad (5)$$

where the split point m is $\frac{n}{2}$. The corresponding uncertainty is denoted as:

$$U'_1 = \{u'_1, u'_2, \dots, u'_m\}, \quad U'_2 = \{u'_{m+1}, u'_{m+2}, \dots, u'_n\}. \quad (6)$$

At this stage, we define the samples corresponding to the elements of U'_1 as a stable set of normal samples, where the mean and variance of U'_1 are denoted by μ_1 and σ_1 , respectively. These statistics represent the uncertainty anchor points for normal samples and uncertainty fluctuations in normal samples. Let $\mathbf{g} = \{g^{(1)}, \dots, g^{(n)}\} \subseteq \{0, 1\}^n$ be a binary vector, where $g^{(i)}$ indicates whether sample i is selected as a training sample. The formula for calculating this vector is as follows:

$$g^{(i)} = \mathbb{I}[a_i \leq a'_m] + \mathbb{I}[a_i \geq a'_{m+1}] \mathbb{I}[u_i \leq \mu_1]. \quad (7)$$

The first term indicates that half of the samples with lower anomaly scores will be used as training samples, while the second term introduces a slight intervention of uncertainty by using the normal anchor point μ_1 to recall some samples with higher scores as training samples. The set of samples selected for training within the batch is denoted as:

$$\mathcal{X}_g = \bigcup_{g^{(i)}=1} x_i. \quad (8)$$

Regular Training Phase. To mitigate this one-sided strong dependency, we integrate uncertainty at this stage. Specifically, for the anomaly estimation scores prior to ranking, we combine them with uncertainty, calculated as follows:

$$A \leftarrow \frac{1}{2} (\text{norm}(A) + \text{norm}(U)). \quad (9)$$

where the norm defaults to min-max normalization. It is important to note that μ_1 and σ_1 are still calculated from the pre-update A' and U' to prevent early leakage, while the remaining components are consistent with the cold-start phase.

3.5. Restoring the Hidden Truth

We follow best practices in FUAD, assuming the noise rate is unknown in advance. To maximize the supervisory signals provided by potential anomaly samples in the training set, a non-destructive outlier exposure method is essential. This method must be capable of operating robustly, even when the noise rate is zero. We synthesize realistic anomalies using normal images and then restore their original appearance from the synthetic anomalies. This approach improves the model's ability to model normal images, which in turn aids in generating fine-grained segmentation maps for anomalous samples. An intuitive illustration of this process is shown in Figure 3.

Anomalous Material Bank Construction. To uncover potential real anomalies, further filtering is required. Let $\mathbf{h} = \{h^{(1)}, \dots, h^{(n)}\} \subseteq \{0, 1\}^n$ be a binary vector, where $h^{(i)}$ indicates whether sample i is selected for constructing the anomaly bank. The calculation formula for this vector is as follows:

$$h^{(i)} = \mathbb{I}[a^{(i)} \geq a_{m+1}] \mathbb{I}[u^{(i)} \geq \mu_1 + \tau \times \sigma_1]. \quad (10)$$

where τ serves as a hyperparameter for tuning outlier detection. A larger value of τ indicates that a sample's uncertainty deviates more from the anchor by multiples of normal fluctuation, thereby being considered a high-confidence anomaly. For each selected anomaly in the minibatch, we construct an anomaly material bank using the method described in Section 3.3:

$$\mathcal{M} = \bigcup_{h^{(i)}=1} \{x_i \in \mathcal{X}_h | M_i^{acc} \geq T_p\}. \quad (11)$$

where T_p is a threshold for selecting the largest region.

Synthetic Anomalies and Optimization Goals. To synthesize real anomalies, we used a PCA-based foreground estimator. By applying PCA to the features generated by the encoder, we obtain a stable object mask. Next, we randomly sample from \mathcal{X}_g . For each sampled image $x_i^* \in \mathcal{X}_g$, we select several anomalous elements from \mathcal{M} , apply random rotations, and paste them onto the foreground region, resulting in the synthetic anomaly image $\tilde{x}_i^* \in \tilde{\mathcal{X}}_g$. Finally, our optimization objective includes both a reconstruction loss and a restoration loss, defined as:

$$\mathcal{L}_{rec.} = \frac{1}{n_1 + n_2} \sum_{i=0}^{n_1} \mathcal{D} \left(F(x_i), \hat{F}(x_i) \right), \quad (12)$$

$$\mathcal{L}_{res.} = \frac{1}{n_1 + n_2} \sum_{i=0}^{n_2} \mathcal{D} \left(F(x_i), \hat{F}(\tilde{x}_i^*) \right), \quad (13)$$

$$\mathcal{L} = \mathcal{L}_{rec.} + \mathcal{L}_{res.}. \quad (14)$$

where $n_1 = |\mathcal{X}_g|$, $n_2 = |\tilde{\mathcal{X}}_g|$ and \mathcal{D} is the hard-mining cosine distance loss function [13].

3.6. Extended Filtering to Datasets

The filtering performance of SSFilter improves continuously during training until it reaches a bottleneck. A well-trained SSFilter acts as an effective sample-level anomaly filter on its own, making it suitable for filtering noisy datasets to produce cleaner datasets. This feature significantly broadens methodological options in practical applications, enabling users to choose the solution best suited to their specific scenario. Specifically, for a trained SSFilter, we perform random iterations over κ_1 epochs and classify a sample as normal if the filter identifies it as normal more than κ_2 times. By default, κ_1 is set to 20, and κ_2 is set to 5.

4. Experiments

4.1. Experimental Settings

Datasets. **Real-IAD** [41] is a large-scale, real-world multi-view dataset designed for industrial anomaly detection. It includes 30 distinct object categories, with 99,721 normal images and 51,329 abnormal images. A sufficiently large dataset enabled the creation of the first comprehensive unsupervised anomaly detection benchmark, which defines four noise levels: $\{0.0, 0.1, 0.2, 0.4\}$. **MVTec AD** [1] is a well-known dataset for industrial anomaly detection, containing more than 5,000 high-resolution images across fifteen object and texture categories.

Implementation Details. By default, the ViT-Small/14 encoder (patch size = 14) is used, pretrained with DINOv2-R [6]. The Noisy Bottleneck has a default dropout rate of 0.2,

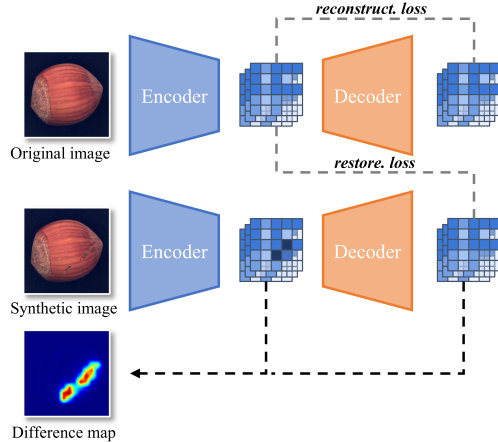


Figure 3. The model restores the original appearance of the object from the real synthetic anomalies.

and the MLP ratio for the MLLA block in the decoder is set to 1.0. The default setting for the number of noise occurrences, K , used to estimate uncertainty is 10. In Equation 1, L_1 is set to $\{0, 3\}$, and L_2 to $\{0, 3, 7\}$, summarizing information from different layers. Additionally, in Equation 10, τ is set to 8. For T_p in Equation 11, the default is the minimum value between 80% of its maximum value and its 99th percentile. In the comparison experiments, unless otherwise specified, the input image size is set to 448^2 , followed by a central crop to 392^2 to ensure that the feature map (28^2) is sufficiently large for anomaly localization. In all ablation study, for efficiency, the input image size is set to 256^2 and then center-cropped to 224^2 , resulting in a decrease in segmentation performance. The StableAdamW optimizer [44] with AMSGrad [36] is used, with a learning rate of 2×10^{-3} and a decay rate of 1×10^{-4} . The network was trained on the Real-IAD dataset for 5,000 iterations using a single NVIDIA RTX 3090 GPU (24GB) with a batch size of 32.

Metrics. Image-level anomaly detection performance is quantified using the Area Under the Receiver Operator Curve (I-AUROC). For anomaly localization, we utilize Area Under the Per-Region Overlap (P-AUPRO). P-AUPRO is designed to treat anomalous regions of various sizes equally, thus providing uniform sensitivity across different anomaly scales.

4.2. Fully Unsupervised Anomaly Detection on Real-IAD

Table 1 presents the experimental results of various state-of-the-art (SOTA) models on the fully unsupervised Real-IAD benchmark. As shown in the table, noise addition in our comparative methods significantly impairs their performance, with degradation accelerating as the noise ratio increases. SoftPatch, which employs a patch-filtering mech-

Table 1. Fully unsupervised anomaly detection and segmentation results with I-AUROC/P-AUPRO(%) on Real-IAD. Methods marked with a superscript † indicate that the training set was filtered using the well-trained SSFilter₄₄₈₃₉₂ model. Subscripts in the table visually depict changes relative to the original experimental data.

Methods	$\alpha = 0.0$	$\alpha = 0.1$	$\alpha = 0.2$	$\alpha = 0.4$	Mean
RD	91.8/94.1	90.2/94.7	89.4/94.8	87.8/94.3	89.8/94.5
Dinomaly	93.9/95.5	91.6/ 96.1	90.0/ 95.5	87.4/ 94.8	90.7/ 95.5
PatchCore	91.9/89.8	90.2/89.0	88.7/88.3	86.3/86.4	89.3/88.4
SoftPatch	91.4/90.7	90.7/91.0	90.1/90.8	88.5/89.8	90.2/90.6
DeSTSeg	91.1/94.5	88.9/93.3	86.3/91.5	82.1/89.8	87.1/92.3
SSFilter ₂₅₆₂₂₄	92.4/90.7	<u>92.3/91.6</u>	<u>92.1/91.5</u>	<u>90.9/91.1</u>	<u>91.9/91.2</u>
SSFilter ₄₄₈₃₉₂	<u>92.5/94.9</u>	92.7/95.2	92.6/95.1	91.8/94.8	92.4/95.0
RD [†]	89.2 _{-2.6} /92.8 _{-1.3}	90.3 _{+0.1} /94.1 _{-0.6}	90.1 _{+0.7} /94.4 _{-0.4}	89.6 _{+1.8} /94.4 _{+0.1}	89.8 _{+0.0} /93.9 _{-0.6}
Dinomaly [†]	92.5 _{-1.4} /95.2 _{-0.3}	92.4 _{+0.8} /95.5 _{-0.6}	91.9 _{+1.9} /95.7 _{+0.2}	90.5 _{+3.1} /95.3 _{+0.5}	91.8 _{+1.1} /95.4 _{-0.1}
PatchCore [†]	90.9 _{-1.0} /89.2 _{-0.6}	90.5 _{+0.3} /89.5 _{+0.5}	90.1 _{+1.4} /89.4 _{+1.1}	88.8 _{+2.5} /88.4 _{+2.0}	90.1 _{+0.8} /89.1 _{+0.7}
SoftPatch [†]	89.9 _{-1.5} /89.4 _{-1.3}	89.8 _{-0.9} /89.9 _{-1.1}	89.7 _{-0.4} /90.3 _{-0.5}	89.3 _{+0.8} /90.2 _{+0.4}	89.7 _{-0.5} /90.0 _{-0.6}
DeSTSeg [†]	89.9 _{-1.2} /94.8 _{+0.3}	90.3 _{+1.4} /95.0 _{+1.7}	90.7 _{+4.4} /94.7 _{+3.2}	89.3 _{+7.2} /93.0 _{+3.2}	90.1 _{+3.0} /94.4 _{+2.1}

anism designed for FUAD, maintains an advantage, though it still experiences a substantial performance drop. The proposed SSFilter performs slightly worse than its baseline model, Dinomaly, in noiseless settings. This performance gap is partly due to the filtering mechanism, which discards some normal samples, and partly due to adjustments made to improve training efficiency. Specifically, we configured the backbone as ViT-S instead of ViT-B, the default in Dinomaly, and reduced the MLP ratio from 4.0 to 1.0. These changes reduced the training time of SSFilter₂₅₆₂₂₄ to approximately match that of standard Dinomaly. While this setup enhanced training and inference speed, it also reduced representation capability.

In addition, SoftPatch, based on PatchCore, also experienced performance degradation compared to its baseline in noise-free settings due to the discard mechanism, underscoring the importance of data-efficient models. At low noise levels (0.1 and 0.2), SSFilter avoids a steep performance drop; in SSFilter₄₄₈₃₉₂, performance under low noise levels even surpasses that in noise-free settings. As noise levels increase, SSFilter’s advantage becomes more pronounced, maintaining robust performance even at a noise setting of 0.4. For SSFilter₂₅₆₂₂₄, the original feature map size is limited to 16^2 , meaning that the interpolated high-resolution feature map provides only coarse anomaly localization, resulting in suboptimal localization performance. Nonetheless, its anomaly detection performance remains comparable to that of SSFilter₄₄₈₃₉₂.

For dataset-level filtering, our practical tests indicate that the actual measured noise rates for the four noise settings in Real-IAD, $\{0.0, 0.1, 0.2, 0.4\}$, are $\{0.0, 0.07, 0.13, 0.26\}$. We calculated the noise rate as the ratio of anomaly samples to the total number of samples in the dataset. Figure 4 and 5

display the noise rate and the normal sample utilization rate of the filtered dataset in comparison to the original dataset, demonstrating the dataset-level filtering capability of our method. Figure 5 indicates that higher noise ratio in the dataset facilitate the model’s ability to learn discriminative information, improving normal sample utilization. Results in Table 1 further show that our method can extend to other approaches. In a noise-free environment, all models experienced a certain degree of performance degradation due to the incompleteness of the training set, reflecting the models’ data efficiency. PatchCore, known for its robust few-shot performance, exhibited the smallest decline. In noisy environments, SoftPatch, specifically designed for FUAD, did not benefit from filtered dataset. However, when noise setting reached 0.4, SoftPatch’s filtering strategy struggled to handle the high noise level, which ultimately resulted in improved performance on the filtered dataset. In most cases, our dataset-level filtering enhanced anomaly detection performance across methods, yielding excellent overall results, though with slight declines in some anomaly localization metrics. For detailed test results for each category, see the appendix.

4.3. Ablation Study

Overall effectiveness comparison of the key elements proposed. We first examine the impact of the proposed key elements on model performance. As shown in Table 2, MLLA directly enhances the model’s overall performance. The patch comparison scoring and uncertainty estimation filtering methods independently improve UAD performance in noisy environments. However, because half of the samples in each batch are discarded in each iteration, these methods result in greater performance degra-

Table 2. **Ablation study on key designs.** **MLLA:** The decoder uses Mamba-Like Linear Attention. **PScoring:** Filtering is performed using the patch comparison scoring mechanism. **UScoreing:** Filtering is performed using uncertainty estimation methods. **URcall:** The uncertainty method participates in the recall of normal samples. **Restoring:** Restore synthesis anomalies.

MLLA	PScoring	UScoreing	URcall	Restoring	$\alpha = 0.0$	$\alpha = 0.4$
×	×	×	×	×	92.5/91.3	86.9/90.8
✓	×	×	×	×	93.0/91.6	87.6/91.3
×	✓	×	×	×	90.8/90.0	88.5/90.2
×	×	✓	×	×	90.7/89.1	88.9/90.6
✓	✓	×	×	×	91.5/90.3	89.1/90.7
✓	✓	×	×	✓	92.2/90.3	89.6/90.0
✓	✓	×	✓	✓	92.5/90.5	90.0/90.7
✓	✓	✓	✓	✓	92.4/90.7	90.9/91.1

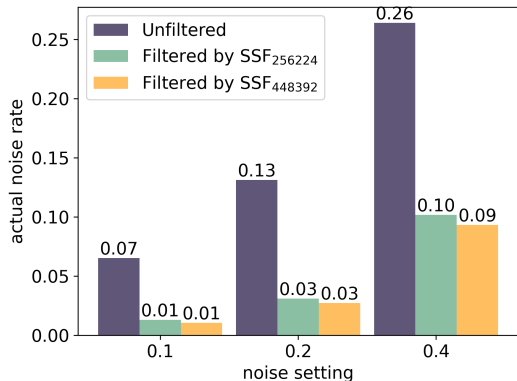


Figure 4. Quantitative results of dataset-level noise filtering are presented.

dation in noise-free environments. When a single filtering strategy is applied, the introduction of MLLA still enhances overall model performance. Furthermore, incorporating the restoring strategy significantly improves performance across varying noise ratios. URcall, defined as the second term in Equation 7, successfully recovers a portion of normal samples from the discarded half, further improving model performance. Finally, by combining the synergistic scoring method outlined in Section 3.4, the robust SSFilter is achieved, allowing the model to attain optimal performance.

Ablation of the patch feature descriptor. In Table 3, we compare the impact of different feature levels on the patch feature descriptor. This experiment uses both the training and testing sets of MVTecAD, with the recall rate of abnormal samples among discarded samples in each batch as the evaluation metric. Given that the number of anomaly samples in MVTecAD is considerably smaller than the number of normal samples, the discard rate is set to 0.3 rather than 0.5 as in other experiments. This setup directly reflects the

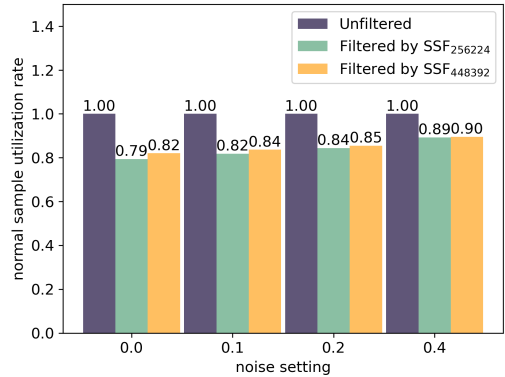


Figure 5. Quantitative results of the utilization rate of normal samples after dataset-level filtering.

Table 3. Ablation studies on patch descriptors.

L_1	L_3	Abnormal Recall
{0}	{-}	0.7831
{3}	{-}	0.8864
{7}	{-}	0.8742
{0,3}	{-}	0.8773
{3,7}	{-}	0.8765
{3}	{0,2,4}	0.8824
{0,3}	{0,2,4}	0.8803
{0}	{0,3,7}	0.8943
{0,3}	{0,3,7}	0.9027

filter’s ability to discard noise samples. The results indicate that performance is limited when using a single layer for the patch feature descriptor, while multi-layer fusion significantly enhances performance.

Additional experiments on hyperparameter robustness and detailed complexity comparison results are provided in the appendix.

5. Conclusions

This paper introduces SSFilter, which is the first method to apply sample-level filtering in noisy unsupervised anomaly detection. The advantage of this filtering approach is its high scalability. SSFilter not only achieves impressive performance in end-to-end fully unsupervised anomaly detection but also allows filtering of the entire dataset using a trained model, thus serving as a bridge between UAD and FUAD methods. We conducted extensive experiments to demonstrate the outstanding performance of our approach.

limitations. Despite SSFilter’s strong performance in noisy scenarios, its filtering mechanism discards some normal samples, causing a degree of performance degradation. Data-efficient unsupervised anomaly detection methods could improve our approach in future work.

References

- [1] Paul Bergmann, Michael Fauser, David Sattlegger, and Carsten Steger. Mvtec ad — a comprehensive real-world dataset for unsupervised anomaly detection. In *2019 IEEE/CVF Conference on Computer Vision and Pattern Recognition (CVPR)*, pages 9584–9592, Long Beach, CA, USA, 2019. IEEE. 6
- [2] Paul Bergmann, Sindy Löwe, Michael Fauser, David Sattlegger, and Carsten Steger. Improving unsupervised defect segmentation by applying structural similarity to autoencoders. In *Proceedings of the 14th International Joint Conference on Computer Vision, Imaging and Computer Graphics Theory and Applications*, pages 372–380, 2019. 2
- [3] Yuanhong Chen, Yu Tian, Guansong Pang, and Gustavo Carneiro. Deep one-class classification via interpolated gaussian descriptor. *Proceedings of the AAAI Conference on Artificial Intelligence*, 36(1):383–392, 2022. 3
- [4] Krzysztof Choromanski, Valerii Likhoshesterov, David Dohan, Xingyou Song, Andreea Gane, Tamas Sarlos, Peter Hawkins, Jared Davis, Afroz Mohiuddin, Lukasz Kaiser, David Belanger, Lucy Colwell, and Adrian Weller. Rethinking attention with performers, 2022. 4
- [5] Simon Damm, Mike Laszkiewicz, Johannes Lederer, and Asja Fischer. Anomalydino: Boosting patch-based few-shot anomaly detection with dinov2, 2024. 2, 4
- [6] Timothée Darcet, Maxime Oquab, Julien Mairal, and Piotr Bojanowski. Vision transformers need registers. <https://arxiv.org/abs/2309.16588v2>, 2023. 3, 6
- [7] Thomas Defard, Aleksandr Setkov, Angelique Loesch, and Romaric Audigier. Padim: A patch distribution modeling framework for anomaly detection and localization. In *Pattern Recognition. ICPR International Workshops and Challenges*, pages 475–489, Cham, 2021. Springer International Publishing. 1, 4
- [8] Hanqiu Deng and Xingyu Li. Anomaly detection via reverse distillation from one-class embedding. In *2022 IEEE/CVF Conference on Computer Vision and Pattern Recognition (CVPR)*, pages 9727–9736, 2022. 1, 2
- [9] Alexey Dosovitskiy, Lucas Beyer, Alexander Kolesnikov, Dirk Weissenborn, Xiaohua Zhai, Thomas Unterthiner, Mostafa Dehghani, Matthias Minderer, Georg Heigold, Sylvain Gelly, Jakob Uszkoreit, and Neil Houlsby. An image is worth 16x16 words: Transformers for image recognition at scale, 2021. 2
- [10] Yarín Gal and Zoubin Ghahramani. Dropout as a bayesian approximation: Representing model uncertainty in deep learning, 2016. 2, 3
- [11] Dong Gong, Lingqiao Liu, Vuong Le, Budhaditya Saha, Moussa Reda Mansour, Svetha Venkatesh, and Anton Van Den Hengel. Memorizing normality to detect anomaly: Memory-augmented deep autoencoder for unsupervised anomaly detection. In *2019 IEEE/CVF International Conference on Computer Vision (ICCV)*, pages 1705–1714, Seoul, Korea (South), 2019. IEEE. 2
- [12] Albert Gu and Tri Dao. Mamba: Linear-time sequence modeling with selective state spaces, 2024. 4
- [13] Jia Guo, Shuai Lu, Lize Jia, Weihang Zhang, and Huiqi Li. Recontrast: Domain-specific anomaly detection via contrastive reconstruction. 2023. 4, 6
- [14] Jia Guo, Shuai Lu, Weihang Zhang, and Huiqi Li. Dino-maly: The less is more philosophy in multi-class unsupervised anomaly detection, 2024. 1, 2, 3, 4
- [15] Bo Han, Quanming Yao, Xingrui Yu, Gang Niu, Miao Xu, Weihua Hu, Ivor W. Tsang, and Masashi Sugiyama. Co-teaching: Robust training of deep neural networks with extremely noisy labels. In *Proceedings of the 32nd International Conference on Neural Information Processing Systems*, pages 8536–8546, Red Hook, NY, USA, 2018. Curran Associates Inc. 2
- [16] Dongchen Han, Ziyi Wang, Zhuofan Xia, Yizeng Han, Yifan Pu, Chunjiang Ge, Jun Song, Shiji Song, Bo Zheng, and Gao Huang. Demystify mamba in vision: A linear attention perspective, 2024. 4
- [17] Haoyang He, Yuhu Bai, Jiangning Zhang, Qingdong He, Hongxu Chen, Zhenye Gan, Chengjie Wang, Xiangtai Li, Guanzhong Tian, and Lei Xie. Mambaad: Exploring state space models for multi-class unsupervised anomaly detection, 2024. 1
- [18] Geoffrey Hinton, Oriol Vinyals, and Jeff Dean. Distilling the knowledge in a neural network, 2015. 2
- [19] Jinchí Huang, Lie Qu, Rongfei Jia, and Binqiang Zhao. O2u-net: A simple noisy label detection approach for deep neural networks. In *2019 IEEE/CVF International Conference on Computer Vision (ICCV)*, pages 3325–3333, Seoul, Korea (South), 2019. IEEE. 2
- [20] Jongheon Jeong, Yang Zou, Taewan Kim, Dongqing Zhang, Avinash Ravichandran, and Onkar Dabeer. Winclip: Zero/few-shot anomaly classification and segmentation. In *Proceedings of the IEEE/CVF Conference on Computer Vision and Pattern Recognition*, pages 19606–19616, 2023. 2
- [21] Xi Jiang, Jianlin Liu, Jinbao Wang, Qiang Nie, Kai Wu, Yong Liu, Chengjie Wang, and Feng Zheng. Softpatch: Unsupervised anomaly detection with noisy data. *Advances in Neural Information Processing Systems*, 35:15433–15445, 2022. 1
- [22] Xi Jiang, Ying Chen, Qiang Nie, Yong Liu, Jianlin Liu, Bin-Bin Gao, Jun Liu, Chengjie Wang, and Feng Zheng. Softpatch: Unsupervised anomaly detection with noisy data, 2024. 3, 1
- [23] Angelos Katharopoulos, Apoorv Vyas, Nikolaos Pappas, and François Fleuret. Transformers are rnns: Fast autoregressive transformers with linear attention, 2020. 2, 4
- [24] Chun-Liang Li, Kihyuk Sohn, Jinsung Yoon, and Tomas Pfister. Cutpaste: Self-supervised learning for anomaly detection and localization, 2021. 2
- [25] Xurui Li, Ziming Huang, Feng Xue, and Yu Zhou. Musc: Zero-shot industrial anomaly classification and segmentation with mutual scoring of the unlabeled images, 2024. 2, 4
- [26] Xiaofan Li, Zhizhong Zhang, Xin Tan, Chengwei Chen, Yanyun Qu, Yuan Xie, and Lizhuang Ma. Promptad: Learning prompts with only normal samples for few-shot anomaly detection, 2024. 4

- [27] Yufei Liang, Jiangning Zhang, Shiwei Zhao, Runze Wu, Yong Liu, and Shuwen Pan. Omni-frequency channel-selection representations for unsupervised anomaly detection. *IEEE Transactions on Image Processing*, 32:4327–4340, 2023. 2
- [28] Wenqian Liu, Runze Li, Meng Zheng, Srikrishna Karanam, Ziyang Wu, Bir Bhanu, Richard J. Radke, and Octavia Camps. Towards visually explaining variational autoencoders. In *2020 IEEE/CVF Conference on Computer Vision and Pattern Recognition (CVPR)*, pages 8639–8648, 2020. 2
- [29] Yang Liu, Hao Cheng, and Kun Zhang. Identifiability of label noise transition matrix. In *Proceedings of the 40th International Conference on Machine Learning*, pages 21475–21496. PMLR, 2023. 2
- [30] Zhikang Liu, Yiming Zhou, Yuansheng Xu, and Zilei Wang. Simplenet: A simple network for image anomaly detection and localization, 2023. 1
- [31] Arian Mousakhan, Thomas Brox, and Jawad Tayyub. Anomaly detection with conditioned denoising diffusion models, 2023. 2
- [32] Maxime Oquab, Timothée Darcet, Théo Moutakanni, Huy Vo, Marc Szafraniec, Vasil Khalidov, Pierre Fernandez, Daniel Haziza, Francisco Massa, Alaaeldin El-Nouby, Mahmoud Assran, Nicolas Ballas, Wojciech Galuba, Russell Howes, Po-Yao Huang, Shang-Wen Li, Ishan Misra, Michael Rabbat, Vasu Sharma, Gabriel Synnaeve, Hu Xu, Hervé Jegou, Julien Mairal, Patrick Labatut, Armand Joulin, and Piotr Bojanowski. DINOv2: Learning robust visual features without supervision, 2024. 3
- [33] Hyunjong Park, Jongyoum Noh, and Bumsub Ham. Learning memory-guided normality for anomaly detection, 2020. 2
- [34] Zhen Qin, Weixuan Sun, Hui Deng, Dongxu Li, Yunshen Wei, Baohong Lv, Junjie Yan, Lingpeng Kong, and Yiran Zhong. cosformer: Rethinking softmax in attention, 2022. 4
- [35] Chen Qiu, Aodong Li, Marius Kloft, Maja Rudolph, and Stephan Mandt. Latent outlier exposure for anomaly detection with contaminated data, 2022. 3
- [36] Sashank J. Reddi, Satyen Kale, and Sanjiv Kumar. On the convergence of adam and beyond, 2019. 6
- [37] Mamshad Nayeem Rizve, Kevin Duarte, Yogesh S. Rawat, and Mubarak Shah. In defense of pseudo-labeling: An uncertainty-aware pseudo-label selection framework for semi-supervised learning, 2021. 3
- [38] Karsten Roth, Latha Pemula, Joaquin Zepeda, Bernhard Schölkopf, Thomas Brox, and Peter Gehler. Towards total recall in industrial anomaly detection, 2022. 1, 3, 4
- [39] Tran Dinh Tien, Anh Tuan Nguyen, Nguyen Hoang Tran, Ta Duc Huy, Soan T.M. Duong, Chanh D. Tr. Nguyen, and Steven Q. H. Truong. Revisiting reverse distillation for anomaly detection. In *2023 IEEE/CVF Conference on Computer Vision and Pattern Recognition (CVPR)*, pages 24511–24520, 2023. 2
- [40] Andreas Veit, Neil Alldrin, Gal Chechik, Ivan Krasin, Abhinav Gupta, and Serge Belongie. Learning from noisy large-scale datasets with minimal supervision, 2017. 2
- [41] Chengjie Wang, Wenbing Zhu, Bin-Bin Gao, Zhenye Gan, Jianning Zhang, Zhihao Gu, Shuguang Qian, Mingang Chen, and Lizhuang Ma. Real-iaD: A real-world multi-view dataset for benchmarking versatile industrial anomaly detection, 2024. 2, 6
- [42] Fengjie Wang, Chengming Liu, Lei Shi, and Pang Haibo. Minimaxad: A lightweight autoencoder for feature-rich anomaly detection, 2024. 1, 2
- [43] Hongxin Wei, Lei Feng, Xiangyu Chen, and Bo An. Combating noisy labels by agreement: A joint training method with co-regularization. In *Proceedings of the IEEE/CVF Conference on Computer Vision and Pattern Recognition*, pages 13726–13735, 2020. 2
- [44] Mitchell Wortsman, Tim Dettmers, Luke Zettlemoyer, Ari Morcos, Ali Farhadi, and Ludwig Schmidt. Stable and low-precision training for large-scale vision-language models, 2023. 6
- [45] Jinggang Yang, Kaiyang Zhou, Yixuan Li, and Ziwei Liu. Generalized out-of-distribution detection: A survey, 2024. 1, 3
- [46] Minghui Yang, Jing Liu, Zhiwei Yang, and Zhaoyang Wu. SlsG: Industrial image anomaly detection by learning better feature embeddings and one-class classification. 2023. 1
- [47] Yu Yao, Tongliang Liu, Mingming Gong, Bo Han, Gang Niu, and Kun Zhang. Instance-dependent label-noise learning under a structural causal model. In *Advances in Neural Information Processing Systems*, pages 4409–4420. Curran Associates, Inc., 2021. 2
- [48] Jinsung Yoon, Kihyuk Sohn, Chun-Liang Li, Sercan O. Arik, Chen-Yu Lee, and Tomas Pfister. Self-supervise, refine, repeat: Improving unsupervised anomaly detection, 2022. 3
- [49] Zhiyuan You, Lei Cui, Yujun Shen, Kai Yang, Xin Lu, Yu Zheng, and Xinyi Le. A unified model for multi-class anomaly detection, 2022. 3
- [50] Vitjan Zavrtanik, Matej Kristan, and Danijel Skocaj. Dræm – a discriminatively trained reconstruction embedding for surface anomaly detection. In *2021 IEEE/CVF International Conference on Computer Vision (ICCV)*, pages 8310–8319, Montreal, QC, Canada, 2021. IEEE. 1, 2
- [51] Xuan Zhang, Shiyu Li, Xi Li, Ping Huang, Jiulong Shan, and Ting Chen. Destseg: Segmentation guided denoising student-teacher for anomaly detection. <https://arxiv.org/abs/2211.11317v2>, 2022. 2, 1
- [52] Xuan Zhang, Shiyu Li, Xi Li, Ping Huang, Jiulong Shan, and Ting Chen. Destseg: Segmentation guided denoising student-teacher for anomaly detection. In *2023 IEEE/CVF Conference on Computer Vision and Pattern Recognition (CVPR)*, pages 3914–3923, 2023. 1
- [53] Zilong Zhang, Zhibin Zhao, Xingwu Zhang, Chuang Sun, and Xuefeng Chen. Industrial anomaly detection with domain shift: A real-world dataset and masked multi-scale reconstruction. *Computers in Industry*, 151(C), 2023. 1
- [54] Qihang Zhou, Guansong Pang, Yu Tian, Shibo He, and Jiming Chen. Anomalyclip: Object-agnostic prompt learning for zero-shot anomaly detection. In *The Twelfth International Conference on Learning Representations*, 2023. 2

A Synergy Scoring Filter for Unsupervised Anomaly Detection with Noisy Data

Supplementary Material

A. More Details of the Experiment.

The methods we utilized in our comparative experiments include RD [8], Dinomaly [14], PatchCore [38], SoftPatch [22] and DeSTSeg [51]. For unmentioned cases, we applied their default configurations, but some specific cases require further clarification. Due to the Real-IAD dataset being an order of magnitude larger than previous datasets, we reduced the epochs of RD from 200 to 50 to minimize unnecessary computations and prevent model overfitting. For PatchCore and SoftPatch, the vast training dataset greatly intensified the storage burden on the Memory Bank, making inference costs excessively high, so we reduced their core set downsampling rate from 0.1 to 0.01. For experiments on DeSTSeg, we adhered to the authors’ experimental guidelines, using a non-rotated configuration for all categories.

B. More Experiments.

We present additional experiments on hyperparameter selection in Table 4, 6, and Table 7, demonstrating strong robustness across all configurations. In the robustness experiments on the threshold T_p in Table 6, we fixed the upper limit at the 99th percentile to avoid excessively small sampling. Therefore, we considered only the maximum value percentage as a hyperparameter. Table 7 details our exploration of methods for selecting the number of materials in a single synthetic image. The methods include random selection from 1 to 3, fixed selection of two, gradual increment with the number of iterations (from 1 to 10), and gradual increment with the number of iterations (from 1 to 5).

To explore the model’s performance under boundary conditions, we reduced the number of normal samples in the training set to be equal to the number of abnormal samples based on the $\alpha = 0.4$ setting, thereby creating a benchmark with a 50% real noise rate. Table 8 presents the experimental results under this benchmark, indicating that our model still outperforms other methods.

Finally, a detailed complexity comparison between SS-Filter and the baseline method, Dinomaly, is presented in Table 5. For training efficiency, SSFilter uses ViT-S as its backbone network by default, instead of the larger, more expressive ViT-B.

C. More Visualized Results.

In Figure 6, we present synthesized anomaly images for several categories in Real-IAD during training, demonstrating that SSFilter effectively leverages potential anomalies in the dataset. Even when applied to clean datasets, synthe-

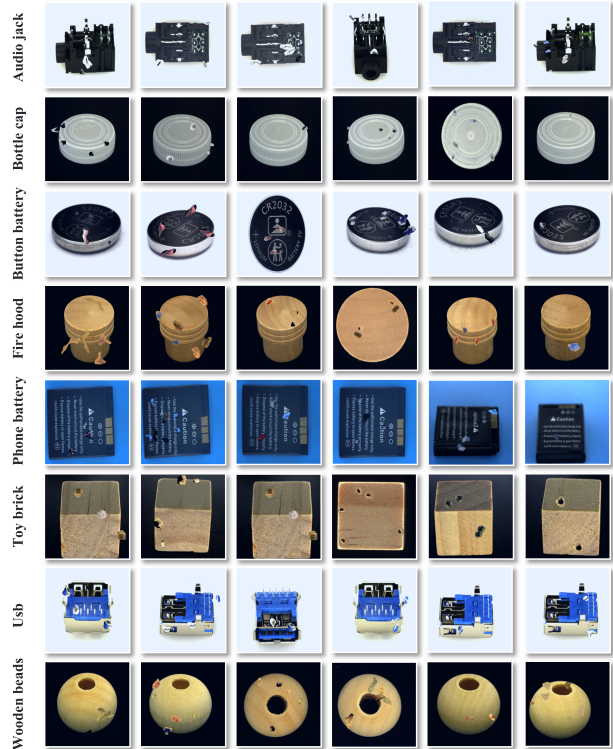


Figure 6. Synthesized image during training.

Table 4. Hyperparameter robustness experiment on the outlier screening hyperparameter τ in Equation 7.

τ	$\alpha = 0.0$	$\alpha = 0.4$
6	92.4/90.7	90.7/90.9
8	92.4/90.4	90.8/91.0
10	92.3/90.3	90.7/91.0

sized anomalies provide valuable segmentation guidance to the model.

D. More Quantitative Results for Each Category.

Tables 9, 10, 11, and 12 present the detailed results of SS-Filter and various state-of-the-art (SoTA) methods for each category under four noise levels, offering comprehensive performance references.

Table 5. Complexity compared with the baseline method. Frames Per Second (FPS) are measured on an NVIDIA RTX 3090 with a batch size of 16. mAD represents the average of the anomaly detection metric (I-AUROC) and the anomaly segmentation metric (P-AUPRO) across the four noise-level benchmarks. Time is the average training time for a single category.

Method	Resolution	Backbone	Params(M)	FLOPs(G)	Time(H)	FPS	mAD
Dinomaly	R448 ² -C392 ²	ViT-B	<u>148.0</u>	114.9	0.7	80	90.7/ 95.5
SSFilter ₂₅₆₂₂₄	R256 ² -C224 ²	ViT-S	31.7	7.8	<u>0.8</u>	638	<u>91.9/91.2</u>
SSFilter ₄₄₈₃₉₂	R448 ² -C392 ²	ViT-S	31.7	<u>26.8</u>	1.7	<u>202</u>	92.4/95.0

Table 6. Hyperparameter robustness experiments for threshold T_p on Real-IAD.

Percentage of maximum	$\alpha = 0.0$	$\alpha = 0.4$
70%	92.1/90.0	90.7/90.7
80%	92.4/90.7	90.9/91.1
90%	92.3/90.6	90.8/91.1

Table 7. Hyperparameter robustness experiment for the number of anomaly materials used in a single synthetic image.

Synthetic number	$\alpha = 0.0$	$\alpha = 0.4$
rand(1,3)	92.3/90.3	90.7/90.8
2	92.4/90.4	90.8/91.0
from 1 to 10	92.3/90.4	90.6/91.3
from 1 to 5	92.4/90.7	90.9/91.1

Table 8. Boundary experiment with 50% real noise ratio.

RD	SoftPatch	SSFilter ₄₄₈₃₉₂
85.9/94.0	86.0/88.4	88.9/93.9

Table 9. FUAD performance (I-AUROC/P-AUPRO&I-AUROC[†]/P-AUPRO[†]) comparisons with state-of-the-art anomaly detection methods on Real-IAD with a noisy ratio of 0.0.

Category	Embedding-based		Synthetic-based	Reconstruction-based			
	PatchCore	SoftPatch	DeSTSeg	RD	Dinomaly	SSFilter ₂₅₆₂₂₄	SSFilter ₄₄₈₃₉₂
Audiojack	90.1/88.1&91.2/88.9	90.6/88.3&90.6/87.4	91.4/94.9&90.0/97.2	90.1/92.6&90.5/92.7	93.4/97.2&92.6/97.0	92.4/89.2&-/-	92.3/94.7&-/-
Bottle Cap	96.8/96.5&96.5/95.7	97.8/98.2&96.9/96.8	94.5/99.8&88.8/99.7	97.1/98.9&96.7/98.6	96.3/99.0&94.7/98.7	97.1/97.3&-/-	95.4/98.6&-/-
Button Battery	86.7/83.7&78.3/73.8	88.4/83.6&78.5/71.8	88.6/92.0&85.1/90.7	88.5/93.5&77.7/85.7	89.0/93.2&80.4/87.8	84.8/81.0&-/-	82.5/87.3&-/-
End Cap	89.0/88.9&89.2/90.5	87.6/90.8&86.5/89.5	85.9/93.3&85.0/93.1	87.0/93.1&86.2/93.2	93.4/97.4&92.6/97.3	89.3/91.6&-/-	90.2/96.3&-/-
Eraser	95.1/95.0&94.5/95.0	94.6/96.5&94.3/95.3	91.6/96.7&94.0/98.8	92.8/95.5&92.9/94.8	95.5/98.6&95.2/98.9	94.9/96.1&-/-	95.0/98.9&-/-
Fire Hood	86.0/86.9&86.9/86.9	86.7/88.6&85.3/88.2	90.1/95.5&91.4/96.5	87.1/93.1&87.2/93.6	90.0/96.6&90.1/96.9	88.5/90.7&-/-	92.3/97.0&-/-
Mint	79.2/70.1&76.8/71.4	76.7/72.1&76.1/70.5	83.7/87.8&79.6/89.9	77.4/84.3&75.6/83.2	88.0/81.2&84.2/84.2	81.0/64.6&-/-	83.3/81.7&-/-
Mounts	90.9/83.9&90.5/85.8	89.8/85.4&89.7/84.9	86.9/87.0&85.5/90.6	91.0/91.0&52.7/72.1	90.7/95.4&90.7/95.0	88.9/90.0&-/-	88.0/96.5&-/-
PCB	94.3/90.8&93.5/88.8	93.5/91.3&92.7/92.2	96.0/95.5&88.7/97.8	94.0/96.1&94.3/96.1	96.8/97.9&96.6/98.0	95.1/92.8&-/-	95.5/97.5&-/-
Phone Battery	93.2/93.5&93.8/93.8	93.4/95.1&92.4/94.8	89.4/95.5&90.6/96.0	93.6/98.5&93.4/98.0	94.8/98.3&94.7/98.5	96.1/96.8&-/-	97.0/98.4&-/-
Plastic Nut	95.5/95.9&92.8/96.3	93.5/96.2&91.4/95.3	87.4/98.6&84.7/98.0	93.8/97.9&91.0/98.0	96.4/98.4&94.1/98.2	94.0/94.1&-/-	93.3/98.0&-/-
Plastic Plug	92.5/91.2&92.5/91.9	92.0/93.1&91.7/92.7	90.2/91.8&83.3/85.6	94.3/96.0&94.0/96.1	94.4/95.4&93.8/95.5	93.0/90.0&-/-	94.1/97.0&-/-
Porcelain Doll	90.3/90.2&90.2/90.5	89.1/91.7&88.7/91.8	90.7/97.7&90.2/97.3	91.6/95.8&90.9/96.2	91.3/97.1&91.3/97.4	92.6/92.2&-/-	93.9/98.2&-/-
Regulator	87.3/91.2&75.5/83.5	84.7/93.1&68.7/79.5	91.9/95.5&88.2/91.7	89.7/97.5&77.8/85.4	92.1/97.8&78.6/92.9	80.5/79.1&-/-	81.4/91.0&-/-
Rolled Strip Base	99.4/98.5&99.3/98.7	99.3/98.7&99.2/98.7	97.7/99.4&98.4/99.7	99.7/99.0&99.7/99.2	99.4/98.6&99.4/98.7	99.6/97.9&-/-	99.2/98.6&-/-
SIM Card Set	98.4/89.5&98.3/90.0	98.2/90.8&98.3/90.7	96.2/98.1&95.7/97.3	97.5/90.9&96.9/91.4	98.2/94.5&98.3/95.8	98.9/92.6&-/-	98.5/96.4&-/-
Switch	96.3/93.1&96.2/92.5	95.5/94.7&95.7/93.8	98.1/97.6&97.3/98.6	96.2/96.9&95.9/96.5	99.0/97.9&98.9/97.6	96.5/95.0&-/-	97.5/95.8&-/-
Tape	98.8/98.2&98.8/98.3	98.7/98.7&98.6/98.5	97.8/99.5&97.6/99.5	98.6/99.0&98.7/99.0	99.1/99.2&99.0/99.3	98.0/98.2&-/-	98.4/98.9&-/-
Terminal Block	97.5/96.7&96.7/96.2	96.2/96.8&96.2/96.9	92.5/98.9&93.6/98.5	98.2/98.5&97.9/98.5	98.2/98.6&98.1/98.8	97.6/97.8&-/-	97.9/99.2&-/-
Toothbrush	89.9/89.6&87.6/88.4	89.2/91.3&87.2/89.3	87.9/81.3&89.4/89.9	85.1/90.4&79.9/87.7	88.6/87.2&84.2/83.9	86.1/85.9&-/-	82.0/84.0&-/-
Toy	89.7/87.2&89.1/87.7	88.4/89.2&88.1/88.0	84.1/93.3&83.7/92.3	89.0/91.4&89.0/91.9	93.0/93.4&92.0/93.3	91.7/86.8&-/-	86.4/84.9&-/-
Toy Brick	83.8/82.4&82.5/81.6	82.9/82.4&81.0/81.5	78.5/83.0&81.1/83.5	75.6/82.8&74.6/85.0	80.2/84.1&79.9/84.0	83.8/80.4&-/-	91.5/92.9&-/-
Transistor1	98.1/96.9&98.1/96.8	97.7/96.9&97.4/97.1	97.3/95.7&96.7/94.2	98.5/98.4&98.4/98.3	98.9/98.3&98.6/98.1	97.9/95.8&-/-	97.0/97.4&-/-
USB	94.9/96.7&95.0/95.9	93.6/96.6&93.7/95.7	94.8/98.3&94.7/99.0	95.3/98.4&95.2/98.5	96.6/98.7&96.3/98.8	94.8/97.6&-/-	92.7/91.6&-/-
USB Adaptor	88.0/82.7&87.5/82.1	88.1/84.3&87.7/84.3	80.5/96.7&77.6/95.2	88.6/82.5&88.2/83.3	90.0/92.0&90.4/92.8	91.6/81.0&-/-	96.0/98.1&-/-
U Block	94.1/95.0&94.0/95.0	93.4/94.5&93.1/95.0	93.4/99.2&92.7/98.7	94.7/98.2&93.8/97.9	95.4/98.0&95.0/97.8	93.5/95.2&-/-	92.7/97.8&-/-
Vcpill	93.2/89.6&93.2/89.2	92.4/89.9&91.3/89.6	93.4/95.5&94.1/94.0	91.7/91.1&91.5/91.7	95.5/96.3&95.2/96.3	93.8/92.6&-/-	93.7/95.1&-/-
Wooden Beads	89.6/83.5&89.1/83.4	90.5/86.3&89.8/87.0	91.3/90.3&90.1/92.5	88.7/90.9&88.9/90.8	91.2/93.2&90.6/94.0	91.9/89.5&-/-	91.1/94.2&-/-
Woodstick	80.7/71.7&80.1/70.7	80.3/71.5&80.7/71.7	92.8/91.3&89.6/91.6	88.1/92.3&87.4/92.1	92.6/94.7&92.3/93.9	91.0/90.9&-/-	92.2/94.7&-/-
Zipper	98.1/96.1&98.0/95.7	97.6/95.7&96.8/94.8	99.1/96.0&99.1/96.1	99.7/98.4&99.3/98.2	99.0/97.8&98.5/97.9	96.3/97.0&-/-	95.3/97.6&-/-
Average All	91.9/89.8&90.9/89.2	91.4/90.7&89.9/89.4	91.1/94.5&89.9/94.8	91.8/94.1&89.2/92.8	93.9/95.5&92.5/95.2	92.4/90.7&-/-	92.5/94.9&-/-

Table 10. FUAD performance (I-AUROC/P-AUPRO&I-AUROC[†]/P-AUPRO[†]) comparisons with state-of-the-art anomaly detection methods on Real-IAD with a noisy ratio of 0.1.

Category	Embedding-based		Synthetic-based	Reconstruction-based			
	PatchCore	SoftPatch	DeSTSeg	RD	Dinomaly	SSFilter ₂₅₆₂₂₄	SSFilter ₄₄₈₃₉₂
Audiojack	89.4/85.9&90.3/88.0	88.9/89.4&89.0/89.5	93.2/96.3&93.4/97.6	89.8/92.7&89.5/93.1	90.2/96.9&92.3/97.2	92.5/90.7&-/-	91.9/94.9&-/-
Bottle Cap	95.3/95.7&96.5/96.7	97.6/98.4&97.2/97.2	95.7/99.9&94.8/99.9	96.0/99.0&96.9/98.8	91.5/98.9&94.5/98.8	97.0/97.3&-/-	96.1/98.6&-/-
Button Battery	80.9/85.0&76.3/79.1	80.6/85.2&73.7/73.8	86.9/87.2&85.3/92.0	85.6/92.9&77.3/87.3	83.7/93.6&79.6/88.0	82.4/84.6&-/-	82.3/89.1&-/-
End Cap	84.1/83.3&87.5/86.1	87.2/89.1&87.1/90.7	82.9/90.6&82.2/89.6	82.3/92.8&84.5/92.9	88.6/96.9&91.1/97.0	88.5/91.6&-/-	90.1/95.7&-/-
Eraser	93.1/95.3&94.3/95.9	94.3/95.6&94.1/96.0	89.9/98.0&93.0/98.7	91.5/96.4&92.3/96.1	94.0/98.7&95.5/99.0	95.6/96.0&-/-	96.2/99.0&-/-
Fire Hood	83.9/85.8&86.6/87.0	85.9/88.6&85.7/88.5	91.6/96.5&93.0/96.1	85.2/93.5&87.2/93.8	88.5/96.8&90.4/96.0	88.9/91.0&-/-	93.1/97.1&-/-
Mint	77.1/71.7&75.5/70.4	75.9/71.9&75.2/72.6	81.8/84.5&81.7/86.9	75.6/85.0&75.8/85.3	83.7/86.4&82.3/85.1	79.9/71.5&-/-	83.0/81.0&-/-
Mounts	93.0/83.7&90.6/86.3	90.7/85.0&89.8/84.3	85.9/93.7&85.9/93.4	92.3/92.5&90.8/92.7	92.3/95.8&90.6/95.1	88.1/89.1&-/-	87.1/95.7&-/-
PCB	92.3/91.1&94.0/91.0	93.1/91.3&92.8/91.1	93.8/97.9&85.5/97.3	93.4/96.2&93.7/96.0	95.6/97.9&96.2/97.8	94.8/92.4&-/-	95.5/96.8&-/-
Phone Battery	93.3/94.8&93.7/94.5	93.0/95.6&92.5/95.7	93.1/96.9&90.0/96.8	93.3/98.9&93.8/98.6	94.9/98.8&95.9/98.8	96.7/97.1&-/-	96.9/98.9&-/-
Plastic Nut	94.2/94.8&93.0/95.1	93.2/96.1&91.9/95.8	90.7/98.7&86.8/98.9	92.8/98.0&90.9/98.0	93.8/98.6&94.5/98.5	94.5/96.1&-/-	94.5/98.0&-/-
Plastic Plug	91.9/92.6&92.3/92.5	92.4/93.3&91.6/92.6	88.8/96.1&89.6/95.9	93.4/96.9&93.6/96.3	93.6/97.3&94.2/96.7	93.4/91.4&-/-	94.2/97.2&-/-
Porcelain Doll	89.4/90.8&90.3/91.1	88.1/92.7&88.9/92.7	80.6/95.1&89.6/97.0	90.7/96.6&91.0/96.5	91.5/98.3&93.0/98.3	92.8/91.8&-/-	94.4/98.1&-/-
Regulator	85.3/91.5&74.2/84.0	82.7/92.5&69.1/79.3	88.4/90.7&86.9/96.2	89.6/98.3&77.6/86.4	86.9/98.8&77.6/93.5	81.4/81.4&-/-	80.8/90.6&-/-
Rolled Strip Base	98.7/98.3&99.3/98.8	99.3/98.8&99.1/98.9	97.3/99.3&98.3/99.7	99.3/99.5&99.7/99.3	97.7/99.0&99.4/98.7	99.5/98.5&-/-	99.4/99.2&-/-
SIM Card Set	96.7/95.2&97.7/94.3	96.8/95.6&97.9/93.6	83.9/94.7&92.5/98.0	95.8/96.4&96.3/94.3	96.6/97.6&98.0/97.5	98.4/94.7&-/-	98.7/97.9&-/-
Switch	94.8/89.1&95.4/92.7	95.3/93.5&95.5/94.0	96.5/93.8&97.3/98.3	96.1/96.1&96.0/96.7	98.5/96.8&98.7/97.4	96.4/95.1&-/-	97.7/95.8&-/-
Tape	97.9/97.6&98.9/98.2	98.7/98.8&98.7/98.6	97.2/99.4&98.1/99.6	98.2/98.8&98.4/98.9	97.9/99.3&98.8/99.2	98.2/98.0&-/-	98.4/99.1&-/-
Terminal Block	96.4/95.8&97.4/96.5	96.6/97.3&96.1/96.7	91.2/97.4&92.1/99.0	98.3/98.9&98.1/98.8	97.6/99.2&98.4/98.8	97.6/97.7&-/-	97.9/99.0&-/-
Toothbrush	89.6/89.0&88.7/89.3	90.1/91.0&88.5/90.4	86.4/76.4&89.7/89.6	81.8/90.8&80.2/89.1	87.6/88.7&86.2/86.9	87.8/86.4&-/-	83.7/85.2&-/-
Toy	85.7/86.2&88.0/87.0	86.9/89.0&88.6/86.9	83.1/89.2&82.7/89.2	85.7/91.7&88.6/92.1	88.7/93.0&92.2/93.5	90.4/89.0&-/-	83.6/84.8&-/-
Toy Brick	80.4/80.6&80.8/80.9	82.3/83.5&80.7/82.4	71.9/80.6&74.3/79.0	71.1/81.2&74.9/84.4	72.3/80.6&76.6/80.4	84.7/81.1&-/-	92.0/93.0&-/-
Transistor1	95.2/94.1&97.7/96.3	95.9/96.1&97.5/96.9	90.1/88.3&95.2/94.9	96.1/98.2&97.8/98.3	97.3/98.1&98.1/98.2	97.1/96.3&-/-	97.3/97.4&-/-
USB	93.2/93.5&95.2/96.8	94.1/95.9&93.6/96.4	93.6/97.8&95.2/96.9	95.3/98.5&95.1/98.4	94.7/98.3&96.2/98.7	95.2/97.6&-/-	93.2/95.5&-/-
USB Adaptor	84.1/82.0&87.1/83.8	87.2/84.5&87.6/84.2	87.2/97.2&87.5/96.2	82.8/91.4&87.2/88.7	86.7/96.6&91.2/96.6	90.8/86.7&-/-	95.9/98.2&-/-
U Block	94.0/94.4&94.5/95.1	94.0/94.5&92.7/94.9	90.1/97.7&94.0/98.7	93.9/98.6&93.5/98.4	94.4/98.3&95.4/98.3	93.6/95.6&-/-	93.2/97.9&-/-
Vcpill	92.4/89.1&93.0/90.5	91.5/89.9&91.5/89.3	91.2/95.5&93.3/92.3	89.2/91.1&90.6/91.2	93.1/95.9&94.9/96.2	93.5/92.7&-/-	93.7/94.9&-/-
Wooden Beads	86.3/80.5&88.8/83.3	89.4/87.1&90.1/85.7	77.5/88.9&89.6/91.1	86.5/90.6&87.4/91.1	88.3/94.0&90.2/94.3	91.7/89.2&-/-	91.6/94.4&-/-
Woodstick	78.9/67.2&80.3/68.5	80.5/73.2&79.8/72.5	92.5/95.3&91.2/93.8	86.0/91.4&87.9/91.7	89.5/94.8&91.5/93.8	91.0/91.0&-/-	92.3/94.5&-/-
Zipper	97.3/95.0&98.2/95.7	97.2/95.5&97.5/95.2	94.7/85.3&99.2/96.2	99.3/98.4&99.6/98.6	98.2/97.7&98.8/97.8	96.3/96.4&-/-	95.3/97.7&-/-
Average All	90.2/89.0&90.5/89.5	90.7/91.0&89.8/89.9	88.9/93.3&90.3/95.0	90.2/94.7&90.3/94.1	91.6/96.1&92.4/95.5	92.3/91.6&-/-	92.7/95.2&-/-

Table 11. FUAD performance (I-AUROC/P-AUPRO&I-AUROC[†]/P-AUPRO[†]) comparisons with state-of-the-art anomaly detection methods on Real-IAD with a noisy ratio of 0.2.

Category	Embedding-based		Synthetic-based	Reconstruction-based			
	PatchCore	SoftPatch	DeSTSeg	RD	Dinomaly	SSFilter ₂₅₆₂₂₄	SSFilter ₄₄₈₃₉₂
Audiojack	87.6/87.7&88.3/87.9	87.7/88.5&88.6/89.0	90.1/94.4&93.3/97.8	88.6/93.2&89.8/92.8	88.6/96.7&90.9/96.7	92.3/89.9&-/-	91.4/94.7&-/-
Bottle Cap	92.9/95.2&95.8/95.3	97.4/98.3&97.0/98.1	92.1/99.2&95.5/99.9	95.2/98/9&96.4/98.6	90.2/98.8&93.4/99.0	96.9/97.1&-/-	95.7/98.5&-/-
Button Battery	80.4/84.1&79.4/84.2	80.6/86.4&77.1/84.2	86.2/92.9&86.9/90.1	84.9/92/8&80.9/90.8	82.0/93.3&80.5/89.9	81.4/82.9&-/-	81.7/89.8&-/-
End Cap	82.7/84.1&85.1/85.4	86.6/90.3&86.0/88.9	79.2/89.7&76.0/90.5	80.5/92/0&83.0/92.6	86.1/96.6&89.6/97.0	86.8/90.0&-/-	88.8/96.4&-/-
Eraser	92.1/95.3&94.0/95.2	94.2/96.6&94.4/95.8	86.6/96.7&92.8/98.1	91.7/97/1&92.2/96.8	92.6/98.6&95.4/98.9	95.1/95.6&-/-	95.9/98.9&-/-
Fire Hood	82.5/85.3&85.8/87.7	85.1/88.2&86.0/87.9	79.0/89.3&87.1/96.1	84.1/93/5&86.3/93.4	87.2/96.4&90.4/96.4	89.4/91.3&-/-	93.6/97.3&-/-
Mint	76.9/70.1&74.6/69.5	75.8/73.3&73.6/70.9	82.7/87.5&83.9/94.1	74.3/86/1&74.7/84.6	81.8/82.0&80.3/83.4	79.8/72.7&-/-	82.5/81.8&-/-
Mounts	92.3/83.8&90.4/84.4	92.4/85.9&89.7/84.8	86.5/94.9&87.5/96.8	92.1/93/8&90.2/92.0	92.1/95.4&90.5/95.2	88.3/89.3&-/-	87.1/95.8&-/-
PCB	92.1/92.0&93.0/92.2	91.9/90.9&92.3/91.7	90.8/93.2&94.3/98.2	92.9/96/2&93.1/95.7	94.5/97.8&95.7/98.0	94.4/91.8&-/-	95.4/96.9&-/-
Phone Battery	90.9/94.1&93.6/95.0	92.8/95.1&92.0/95.3	91.8/96.7&91.8/97.1	92.2/98/5&93.4/98.8	93.0/98.8&95.9/98.8	96.7/98.1&-/-	97.1/98.8&-/-
Plastic Nut	93.1/94.7&93.8/95.6	93.1/96.2&91.7/95.1	85.1/96.6&87.5/96.6	91.7/98/2&92.5/97.9	92.3/98.2&94.4/98.7	94.4/96.0&-/-	94.8/97.7&-/-
Plastic Plug	90.6/91.9&92.1/92.2	92.3/93.3&91.5/91.7	84.4/94.0&91.0/96.8	91.8/96/8&93.1/96.9	92.3/97.1&93.9/97.4	93.5/91.1&-/-	94.1/97.3&-/-
Porcelain Doll	87.7/91.2&89.2/91.9	87.7/92.1&88.7/92.9	86.9/96.1&89.7/97.9	90.3/96/9&91.2/96.3	90.6/98.2&92.8/98.5	92.5/92.0&-/-	93.8/98.2&-/-
Regulator	82.9/90.4&77.1/88.0	83.4/94.4&71.0/83.9	90.5/95.2&87.8/85.8	88.4/98/4&82.2/93.3	85.0/98.5&79.6/96.0	81.6/87.6&-/-	82.6/92.2&-/-
Rolled Strip Base	96.7/97.5&99.2/98.6	98.4/98.3&99.2/98.9	95.0/99.1&97.8/99.1	98.5/99/5&99.7/99.3	95.6/98.8&99.1/98.7	99.5/98.6&-/-	99.4/99.3&-/-
SIM Card Set	95.8/94.9&97.5/94.7	96.2/95.2&97.6/93.8	90.8/98.1&95.6/99.0	95.3/96/7&96.1/94.8	95.7/97.8&97.9/97.6	98.3/94.3&-/-	98.8/97.9&-/-
Switch	94.0/89.2&95.1/93.3	95.7/93.8&95.6/93.7	90.9/91.8&96.9/96.5	95.8/95/6&95.7/96.5	98.0/96.4&98.2/97.3	96.1/94.7&-/-	97.5/95.5&-/-
Tape	97.2/98.0&98.9/98.5	98.4/98.5&98.7/98.6	94.3/98.5&98.6/99.7	97.7/99/0&98.6/98.9	96.9/99.0&98.9/99.2	98.2/98.0&-/-	98.4/99.0&-/-
Terminal Block	95.3/94.5&97.2/96.1	96.8/96.9&96.3/96.9	90.2/98.0&96.0/99.5	98.0/99/1&98.5/99.0	96.7/99.1&98.3/98.8	97.5/97.6&-/-	98.3/99.0&-/-
Toothbrush	87.4/88.3&87.4/86.9	89.3/89.9&88.4/89.9	78.8/67.2&86.5/82.1	80.7/90/7&80.0/89.1	84.5/87.8&83.8/85.5	85.8/86.8&-/-	83.0/84.7&-/-
Toy	82.6/85.3&85.4/85.0	85.9/87.8&86.1/88.6	70.0/58.6&81.2/88.8	84.6/92/2&87.2/92.8	85.2/92.4&90.8/93.5	89.8/87.3&-/-	84.0/82.8&-/-
Toy Brick	78.3/78.1&80.9/79.3	80.2/82.8&81.3/83.6	69.0/77.8&76.6/78.6	71.2/81/2&73.0/82.5	68.5/78.4&75.0/82.3	85.0/79.4&-/-	91.2/91.0&-/-
Transistor1	93.4/91.3&97.0/95.2	94.3/95.1&97.0/96.8	87.0/90.4&96.1/94.5	94.7/97/8&97.2/98.1	95.6/97.7&97.4/97.8	96.7/96.2&-/-	97.1/97.2&-/-
USB	92.0/92.5&94.4/95.3	93.2/95.8&93.9/96.5	90.8/96.6&95.7/98.7	94.5/98/3&95.0/98.5	94.1/98.3&96.5/98.6	95.2/97.1&-/-	93.3/95.1&-/-
USB Adaptor	82.6/81.3&85.8/82.4	85.2/85.5&86.8/83.8	86.2/96.8&87.3/96.9	80.8/91/1&85.3/90.8	83.3/96.9&89.3/96.6	90.7/86.9&-/-	96.4/98.1&-/-
U Block	93.3/94.6&94.1/94.5	94.2/95.9&93.6/95.3	82.2/96.1&94.0/99.0	93.4/98/5&93.4/98.2	92.7/98.2&94.8/98.5	93.6/95.8&-/-	92.9/97.6&-/-
Vcpill	90.6/87.7&92.0/89.7	90.3/89.0&91.1/89.4	85.9/92.3&94.5/92.8	88.2/90/7&91.0/91.4	92.4/95.2&94.0/95.7	93.3/92.0&-/-	93.4/95.2&-/-
Wooden Beads	85.7/80.6&87.9/82.3	87.3/85.4&89.2/86.7	82.8/87.2&88.5/91.9	85.4/90/6&87.4/91.0	86.3/93.1&89.4/93.2	91.4/88.6&-/-	91.0/94.2&-/-
Woodstick	75.5/63.0&79.3/69.6	81.1/69.9&79.4/72.0	87.9/89.9&91.0/91.3	85.6/90/8&87.6/91.6	87.3/91.4&90.9/95.4	91.0/90.1&-/-	92.4/93.8&-/-
Zipper	96.4/93.9&98.0/95.9	96.5/95.4&97.5/95.6	94.7/90.3&98.8/96.0	99.2/98/3&99.6/98.6	97.9/97.4&98.9/98.2	96.8/96.9&-/-	96.2/98.1&-/-
Average All	88.7/88.3&90.1/89.4	90.1/90.8&89.7/90.3	86.3/91.5&90.7/94.7	89.4/94.8&90.1/94.4	90.0/95.5&91.9/95.7	92.1/91.5&-/-	92.6/95.1&-/-

Table 12. FUAD performance (I-AUROC/P-AUPRO&I-AUROC[†]/P-AUPRO[†]) comparisons with state-of-the-art anomaly detection methods on Real-IAD with a noisy ratio of 0.4.

Category	Embedding-based		Synthetic-based	Reconstruction-based			
	PatchCore	SoftPatch	DeSTSeg	RD	Dinomaly	SSFilter ₂₅₆₂₂₄	SSFilter ₄₄₈₃₉₂
Audiojack	85.3/81.3&86.6/86.7	85.6/88.3&86.4/88.6	83.2/95.4&90.3/95.4	85.9/92.5&87.7/92.7	83.7/96.0&87.7/96.1	90.6/89.5&-/-	88.4/94.2&-/-
Bottle Cap	91.6/94.9&95.6/96.3	96.8/97.8&97.6/98.2	85.9/99.0&95.2/99.6	92.7/98.5&96.7/98.7	85.6/97.9&92.0/98.5	96.3/96.9&-/-	95.3/98.2&-/-
Button Battery	77.7/83.3&77.4/84.3	77.1/84.9&77.4/84.7	74.7/88.5&85.9/91.0	82.6/92.5&82.2/92.2	78.1/91.4&79.1/92.2	79.7/86.2&-/-	78.8/89.6&-/-
End Cap	79.2/80.2&82.8/83.3	82.9/86.2&85.3/88.8	77.4/83.2&75.4/90.4	77.5/91.4&81.8/91.8	82.9/96.3&87.2/96.4	84.9/88.1&-/-	88.0/95.9&-/-
Eraser	90.5/93.0&93.6/94.1	93.4/96.4&94.0/96.0	74.4/80.3&93.7/99.0	88.6/97.1&91.5/95.5	89.4/97.8&94.5/98.9	95.4/94.9&-/-	96.3/99.0&-/-
Fire Hood	80.3/82.4&84.9/85.7	84.0/87.9&85.4/87.8	89.1/96.2&92.1/96.5	83.7/92.4&85.8/92.8	85.8/95.5&89.7/96.0	87.2/89.7&-/-	93.1/97.1&-/-
Mint	72.5/69.8&75.8/69.7	74.7/73.2&75.1/70.1	74.2/84.5&79.9/82.7	70.7/83.6&75.5/86.1	78.6/84.7&79.8/84.3	78.1/72.1&-/-	81.7/81.0&-/-
Mounts	90.7/82.4&91.7/82.4	90.9/84.2&88.9/84.7	77.1/88.5&87.1/97.6	91.1/94.4&90.1/92.1	90.7/95.4&91.1/95.2	87.4/88.8&-/-	86.9/95.9&-/-
PCB	90.5/88.2&91.2/90.7	90.0/90.1&91.0/90.3	78.3/95.6&90.7/98.5	91.9/95.6&92.6/95.4	92.8/97.9&94.1/97.8	93.1/92.6&-/-	94.5/97.1&-/-
Phone Battery	88.1/90.7&92.5/94.4	91.0/95.3&91.7/96.0	87.5/91.3&93.0/96.7	90.6/98.6&93.1/98.6	91.2/98.7&94.9/98.9	96.8/98.0&-/-	97.0/98.5&-/-
Plastic Nut	92.4/93.3&93.6/95.1	91.4/95.8&91.1/95.4	85.6/98.2&87.7/98.8	90.2/98.1&92.2/98.1	90.3/97.9&93.9/98.8	94.1/96.1&-/-	95.1/97.7&-/-
Plastic Plug	89.7/91.1&92.3/93.0	91.8/93.4&91.1/92.6	77.5/92.8&90.4/92.9	91.6/97.2&93.2/96.6	90.3/96.7&93.5/97.1	93.0/93.6&-/-	93.7/97.4&-/-
Porcelain Doll	85.2/89.5&88.8/91.2	86.3/91.1&87.8/91.9	81.2/96.8&88.1/94.9	89.5/96.9&90.7/96.8	88.3/97.8&92.1/98.3	92.0/91.6&-/-	93.6/97.9&-/-
Regulator	81.2/90.6&78.4/88.8	82.8/91.4&76.2/89.8	87.2/96.6&83.5/85.0	88.4/98.2&85.1/97.1	82.4/98.3&80.5/97.8	81.5/88.4&-/-	81.9/93.9&-/-
Rolled Strip Base	94.0/96.4&96.0/96.9	95.1/97.1&97.6/97.8	92.2/97.4&94.4/91.9	97.4/99.5&97.9/99.2	92.4/98.5&95.7/98.5	97.5/98.0&-/-	98.0/98.9&-/-
SIM Card Set	94.0/94.4&96.4/95.0	95.3/95.6&96.6/95.8	88.7/98.1&96.3/98.7	93.2/96.6&95.2/95.3	94.1/97.8&96.9/97.8	97.3/94.6&-/-	98.3/96.9&-/-
Switch	91.9/86.2&95.1/89.9	94.9/91.3&95.4/93.1	88.8/89.7&96.0/95.1	93.9/94.3&95.5/95.6	96.5/95.2&97.3/96.3	95.4/94.4&-/-	96.9/94.8&-/-
Tape	96.3/97.1&98.5/97.9	97.3/98.3&98.7/98.6	93.1/98.5&98.3/99.7	96.8/98.7&98.0/98.8	95.7/98.9&98.6/99.3	98.1/97.8&-/-	98.6/98.9&-/-
Terminal Block	91.4/92.8&95.2/94.3	96.0/97.3&96.1/96.4	85.7/99.3&95.3/99.4	96.7/99.1&97.8/99.0	94.9/99.0&97.4/98.9	97.5/97.3&-/-	97.9/99.0&-/-
Toothbrush	85.1/86.6&84.8/85.9	86.9/90.3&86.9/88.3	78.5/70.9&79.1/69.4	78.1/89.5&76.6/87.8	81.5/85.8&81.8/84.5	83.0/85.1&-/-	79.9/80.9&-/-
Toy	75.9/82.1&79.8/82.1	83.5/87.0&83.9/86.6	79.1/83.6&80.6/85.8	81.0/91.6&85.9/92.0	81.0/90.0&84.9/91.2	88.1/86.3&-/-	80.1/81.8&-/-
Toy Brick	76.2/77.3&76.7/77.6	78.2/80.3&79.1/81.1	65.0/68.7&73.1/79.2	68.5/78.3&71.4/81.3	64.9/73.3&70.3/77.6	78.6/71.9&-/-	90.7/92.0&-/-
Transistor1	89.8/85.5&94.4/92.4	90.7/91.7&95.9/96.2	77.0/70.5&89.1/86.9	91.6/97.3&95.3/97.8	92.2/96.7&95.1/97.1	93.7/94.9&-/-	95.7/97.1&-/-
USB	88.1/88.9&92.3/92.7	92.5/96.0&93.2/95.7	79.6/93.9&94.9/98.4	93.1/98.3&94.3/98.1	91.6/97.8&95.3/98.4	95.0/97.2&-/-	92.1/95.1&-/-
USB Adaptor	78.0/81.9&82.2/82.3	82.7/83.4&85.7/84.3	71.1/88.8&87.3/97.0	79.0/90.6&83.2/91.1	78.6/95.9&86.0/96.3	89.1/86.2&-/-	96.3/97.9&-/-
U Block	92.3/94.2&93.4/94.8	93.2/94.4&93.5/96.0	89.0/98.4&94.5/99.0	93.1/98.6&93.5/98.4	91.7/98.1&94.4/98.5	93.5/95.8&-/-	93.0/97.6&-/-
Vcpill	89.6/87.9&90.8/88.9	89.8/88.7&90.5/88.3	81.2/80.0&94.1/94.1	87.1/89.8&91.1/90.8	90.0/94.3&93.0/94.8	92.5/91.7&-/-	92.7/94.8&-/-
Wooden Beads	83.2/75.9&88.4/82.3	86.2/83.6&88.7/85.6	79.2/87.9&90.1/87.2	83.5/90.3&85.8/91.1	84.6/92.8&88.7/93.8	90.5/90.3&-/-	90.7/93.8&-/-
Woodstick	74.6/61.1&78.5/67.9	79.5/68.9&80.3/71.0	88.7/92.0&87.7/94.2	86.3/90.6&88.0/91.5	85.4/91.8&89.5/92.0	89.7/89.9&-/-	91.6/94.6&-/-
Zipper	94.7/92.2&97.8/94.8	95.0/94.2&97.1/94.9	91.0/88.8&96.0/94.3	98.6/98.1&99.6/98.4	97.0/96.8&98.7/97.5	97.8/96.5&-/-	97.6/96.9&-/-
Average All	86.3/86.4&88.8/88.4	88.5/89.8&89.3/90.2	82.1/89.8&89.3/93.0	87.8/94.3&89.6/94.4	87.4/94.8&90.5/95.3	90.9/91.1&-/-	91.8/94.8&-/-